Theoretical and Mathematical Physics, **182**(1): 1–22 (2015)

HOLOGRAPHIC DUAL OF A CONICAL DEFECT

© **I. Ya. Arefeva*** **and A. A. Bagrov†**

We consider a moving conical defect in the pure AdS_3 space–time and calculate two-point correlation functions of a corresponding two-dimensional boundary quantum field theory in the geodesic approximation. We show that the presence of the defect leads to a gravitational lensing of geodesics, and this results in a finite number of similar terms in the Green's function that correspond to winding geodesics in the bulk around the conical singularity. We show that for the quantized deficit angle $\gamma = \pi/2n$, the lensing produces domain wall excitations in the spectrum of the boundary theory.

Keywords: AdS/CFT duality, conical defect, holographic duality

1. Introduction

The AdS/CFT correspondence [1] is now regarded as the most powerful and universal tool for analyzing nonperturbative phenomena in quantum field theory in the contexts of both high energy physics [2], [3] and condensed matter physics [4]. The power of this duality is mainly rooted in its flexibility: the AdS/CFT dictionary seems applicable to a very broad class of metrics with AdS asymptotic forms and can hence be used to study the properties of nonconformal quantum field theories at a nonzero temperature, at a nonzero chemical potential, for potential-modulated external lattices containing explicit infrared cutoffs, and so on.

Among other possibilities, one natural and simple way to deform a conformal symmetry is to introduce topological defects in the bulk of the AdS space. Here, we consider a conical defect in AdS_3 produced by a moving massive particle (Lorentz transform of the Deser–'t Hooft metric [5], [6]) and calculate two-point correlation functions in the dual (1+1)-dimensional theory in the geodesic approximation. Analyzing correlation functions on conical defects has long been a research subject (see [7] and the references therein). Here, we deal not with real defects in the boundary field theory but with defects in the auxiliary holographic space–time. The consideration of such conical defects was started in [8]. In a certain sense, our analysis is complementary to the considerations in [9], where a cosmic string in the AdS_4 space orthogonal to the conformal boundary of the space–time and "penetrating" it was considered. The influence of cosmic membranes in AdS_5 on observables in the four-dimensional boundary field theory was investigated in [10] in the context of phenomenological extra-dimensional scenarios. Models of dS spaces with conical defects are related to cosmic strings in an expanding universe.

This paper is organized as follows. In Sec. 2, we define the basic objects needed for the analysis. We first formulate an algebraic representation of the AdS_3 space–time, both empty and with massive particles. We recall the basic notions of the geodesic approximation in holography, which we use to calculate two-point correlation functions in the boundary theory. In Sec. 3, we use this approximation to analyze the theory dual to a conical defect in the bulk (we consider both the static case and the case of a defect moving along

*Steklov Mathematical Institute, RAS, Moscow, Russia, e-mail: arefeva@mi.ras.ru.

†Instituut-Lorentz for Theoretical Physics, Leiden University, Leiden, The Netherlands, e-mail: bagrov@lorentz.leidenuniv.nl.

Prepared from an English manuscript submitted by the authors; for the Russian version, see *Teoreticheskaya i Matematicheskaya Fizika*, Vol. 182, No. 1, pp. 3–27, January, 2014. Original article submitted June 24, 2014.

a circular orbit). In Sec. 4, we consider the momentum representation of the obtained correlation functions. In Sec. 5, we briefly discuss the obtained results and also indicate how our consideration possibly relates to calculating the entanglement entropy in nonconformal two-dimensional systems.

2. Basic objects

2.1. Algebraic representation of AdS_3. The most convenient language for achieving our purposes is the algebraic description of the AdS_3 space–time based on the fact that this space is locally isometric to a covering of the $SL(2,\mathbb{R})$ group manifold. Using this isometry, we can represent both points and transformations of the space–time corresponding to the insertion of matter sources in the bulk as real 2×2 matrices. Many problems are thus reducible to solving simple matrix equations. Here, we actively use the techniques developed in [11]–[13] and adapted to this description.

The AdS_3 space–time can be covered by a global coordinate chart (τ,χ,ϕ), where $\chi\geq0$, $\phi\simeq\phi+2\pi$, and $\tau\in(-\infty,\infty)$ (the so-called barrel coordinates [14]). The metric of a space with these coordinates has the form

$$ds^2=d\chi^2+\sinh^2\chi\,d\phi^2-\cosh^2\chi\,d\tau^2. \tag{1}$$

We also use the Poincaré disk coordinate r, related to ρ by $r=\tanh(\chi/2)$ and leading to a metric of the form

$$ds^2=-\left(\frac{1+r^2}{1-r^2}\right)^2d\tau^2+\left(\frac{2}{1-r^2}\right)^2(dr^2+r^2\,d\phi^2),\quad r<1. \tag{2}$$

In terms of the barrel coordinates or the r coordinates, the $SL(2,\mathbb{R})$ group manifold can be parameterized by

$$\mathbf{x}=\cosh\chi\,\mathbf{\Omega}(\tau)+\sinh\chi\,\mathbf{\Gamma}(\phi)=\frac{1+r^2}{1-r^2}\,\mathbf{\Omega}(\tau)+\frac{2r}{1-r^2}\,\mathbf{\Gamma}(\phi),$$

where

$$\mathbf{\Omega}(\tau)=\cos\tau\,\mathbf{1}+\sin\tau\,\gamma_0,\qquad\mathbf{\Gamma}(\phi)=\cos\phi\,\gamma_1+\sin\phi\,\gamma_2. \tag{3}$$

Here, $\mathbf{1}$ is the unit matrix, and the gamma matrices form an orthonormal basis of the associated Lie algebra $\mathfrak{sl}(2)$ of traceless matrices,

$$\gamma_0=\begin{pmatrix}0&1\\-1&0\end{pmatrix},\qquad\gamma_1=\begin{pmatrix}0&1\\1&0\end{pmatrix},\qquad\gamma_2=\begin{pmatrix}1&0\\0&-1\end{pmatrix}.$$

The matrices $\mathbf{\Omega}(\tau)$ and $\mathbf{\Gamma}(\phi)$ satisfy the relations

$$\mathbf{\Omega}(\tau)\mathbf{\Omega}(\tau')=\mathbf{\Omega}(\tau+\tau'),\qquad\mathbf{\Omega}(\tau)\mathbf{\Gamma}(\phi')=\mathbf{\Gamma}(\tau+\phi'),$$
$$\mathbf{\Gamma}(\phi)\mathbf{\Gamma}(\phi')=\mathbf{\Omega}(\phi-\phi'),\qquad\mathbf{\Gamma}(\phi)\mathbf{\Omega}(\tau')=\mathbf{\Gamma}(\phi-\tau').$$

Metric (1) is then just the Cartan–Killing metric

$$ds^2=\frac{1}{2}\mathrm{Tr}(\mathbf{x}^{-1}\,d\mathbf{x}\,\mathbf{x}^{-1}\,d\mathbf{x}),$$

2.2. Point particle in $\mathbf{AdS_3}$. As shown by Deser and 't Hooft [6], [5], the effect of a massive point particle in three-dimensional Einstein gravity is that preserving the local metric unchanged, it produces a conical singularity, whose holonomy $\mathbf{u}$ is defined by the mass of the particle and its kinetic characteristics [12]. For particle masses below a certain threshold, this effect appears the same both in a flat space and in the presence of a cosmological constant.

More precisely, placing a stationary pointlike massive particle in the (2+1)-dimensional Minkowski space results in cutting out a wedge from the original space, and the angular deficit is proportional to the particle mass. The faces of the wedge are identified, which produces a conical singularity at the particle position and leaves the rest of the space flat.

If the particle moves along a certain nontrivial trajectory, then points on the faces of the wedge emerging from the particle worldline must be identified at equal times in the particle rest frame. The space–time in the frame of an external observer then undergoes an isometry (which is also a Lorentz transformation) whose fixed subset is the particle worldline.

To obtain a similar space of constant curvature containing a pointlike particle, we use the "cut-and-glue" procedure described below.

2.2.1. Stationary pointlike particle in $\mathbf{AdS_3}$. We consider a stationary pointlike mass located at the coordinate origin $\chi = 0$. In this case, in each slice of constant time τ, a wedge bounded by two spacelike geodesics emerging from the origin is removed, and the geodesics are identified. The angle 2γ between the faces of the wedge is proportional to the particle mass.

The mathematical formulation of this procedure involves parameterizing the front face (1-face) of the wedge by matrices of the form

$$\mathbf{x}_{\text{1-face}} = \cosh\chi\,\mathbf{\Omega}(\beta) + \sinh\chi\,\mathbf{\Gamma}(-\gamma), \tag{4}$$

depending on two variables χ and β, $\chi \geq 0$, $-\infty \leq \beta \leq \infty$. The quantity 2γ is fixed. The back face (2-face) is given by

$$\mathbf{x}_{\text{2-face}} = \cosh\chi\,\mathbf{\Omega}(\beta) + \sinh\chi\,\mathbf{\Gamma}(\gamma). \tag{5}$$

These two wedges are related by the transformation

$$\mathbf{x}_{\text{2-face}} = B^{-1}\mathbf{x}_{\text{1-face}}B, \tag{6}$$

where $B = \mathbf{\Omega}(-\gamma)$ and $\mathbf{\Omega}$ is given by (3). Obviously, the line $\chi = 0$ is invariant under this transformation in the sense that the matrix

$$\mathbf{x}_0(\beta) \equiv \mathbf{\Omega}(\beta) \tag{7}$$

satisfies the identity

$$B^{-1}\mathbf{x}_0 B = \mathbf{x}_0. \tag{8}$$

We can say that the transformation B with the worldline of a stationary particle as its locus of fixed points is the mathematical representation of a pointlike source in three-dimensional gravity.

For our future goals related to constructing a holographic dual description of the Gott time machine (the next paper is devoted to this question), it is useful to discuss the following nuance. We note that matrix representation (4) and (5) of the wedge faces is not unique. Without violating conditions (6) and (8), we can set

$$\mathbf{x}_{\text{1-face}} = \cosh\chi\,\mathbf{\Omega}(\beta) + \sinh\chi\,\mathbf{\Gamma}(\beta-\gamma), \tag{9}$$

$$\mathbf{x}_{\text{2-face}} = \cosh\chi\,\mathbf{\Omega}(\beta) + \sinh\chi\,\mathbf{\Gamma}(\beta+\gamma), \tag{10}$$

and the wedge faces can then be represented as rotating straight lines sweeping a helix in the space–time.

2.2.2. Moving conical defect. In this section, we discuss the space–time produced by a massive particle moving in the AdS_3 space in a definite way, namely, orbiting a center of the AdS_3 space in a circular orbit.[1] This space–time is an essential ingredient of the AdS modification of the Gott time machine [15] and can be obtained by a boost transformation of a single massive pointlike particle located in the center of the AdS_3 space. To find the corresponding identification matrix, we must find a matrix that transforms rest particle matrix (7) into the matrix describing the particle moving along the spiral

$$\mathbf{x}_{\text{spiral}}(\beta,\psi_0)=\cosh\psi_0\,\mathbf{\Omega}(\beta)+\sinh\psi_0\,\mathbf{\Gamma}(\beta), \tag{11}$$

where β is a continuous parameter and ψ_0 is fixed. The spiral $\mathbf{x}_{\text{spiral}}$ is given by the Lorentz transformation $\mathbf{x}_{\text{spiral}}=\mathbf{x}_0\mathbf{L}(\psi_0)$, where

$$\mathbf{L}(\psi_0)=\cosh\psi_0\,\mathbf{\Omega}(0)+\sinh\psi_0\,\mathbf{\Gamma}(0). \tag{12}$$

Acting on first face (9) with Lorentz transformation (12), we obtain the set of matrices describing the leading face (1-mov-face) of the moving wedge:

$$\mathbf{x}_{\text{1-mov-face}}=\mathbf{x}_{\text{1-face}}\,\mathbf{L}(\psi_0). \tag{13}$$

Parameterizing the leading face as

$$\mathbf{x}_{\text{1-mov-face}}=\cosh\chi^{(1)}\,\mathbf{\Omega}(t^{(1)})+\sinh\chi^{(1)}\,\mathbf{\Gamma}(\phi^{(1)}),$$

we obtain the formulas for $t^{(1)}$, $\phi^{(1)}$, and $\chi^{(1)}$,

$$\tan t^{(1)}=\frac{\tan\beta-\tanh\chi\tanh\psi_0(\sin\gamma-\tan\beta\cos\gamma)}{1+\tanh\chi\tanh\psi_0(\cos\gamma+\tan\beta\sin\gamma)},$$

$$\tan\phi^{(1)}=\frac{\tanh\chi(-\sin\gamma+\tan\beta\cos\gamma)+\tanh\psi_0\tan\beta}{\tanh\chi(\cos\gamma+\tan\beta\sin\gamma)+\tanh\psi_0},$$

$$\begin{aligned}\cosh\chi^{(1)}=\cosh\chi\cosh\psi_0\cos\beta\,\times\\ \times\big[\big(\tan\beta+\tanh\chi\tanh\psi_0(\tan\beta\cos\gamma-\sin\gamma)\big)^2+\\ +\big(1+\tanh\chi\tanh\psi_0(\cos\gamma+\tan\beta\sin\gamma)\big)^2\big]^{1/2}.\end{aligned}$$

The trailing face (2-mov-face) is

$$\mathbf{x}_{\text{2-mov-face}}=\mathbf{x}_{\text{2-face}}\mathbf{L}(\psi_0),$$

and we have

$$\mathbf{x}_{\text{2-mov-face}}=\mathbf{\Omega}(\gamma)\,\mathbf{x}_{\text{1-mov-face}}\,\mathbf{\Omega}_{\mathbf{L}}(-\gamma,\psi_0).$$

Here, we use (13) and introduce the notation

$$\mathbf{\Omega}_{\mathbf{L}}(-\gamma,\psi_0)\equiv\mathbf{L}^{-1}(\psi_0)\mathbf{\Omega}(-\gamma)\mathbf{L}(\psi_0).$$

Therefore, the identification formula has the simple form

$$\mathbf{y}'=\mathbf{\Omega}(\gamma)\mathbf{y}\mathbf{\Omega}_{\mathbf{L}}(-\gamma,\psi_0). \tag{14}$$

[1] Of course, because the AdS space is maximally symmetric, we can consider any point its center.

It can be easily verified that spiral (11) is invariant under isometry (14),

$$\mathbf{x}'_{\text{spiral}} = \mathbf{\Omega}(\gamma)\mathbf{x}_{\text{spiral}}(\psi_0)\mathbf{\Omega_L}(-\gamma,\psi_0) = \mathbf{x}_{\text{spiral}}.$$

On the AdS_3 boundary, we have

$$\tan\phi_{1,2} = \frac{\sin\beta\tanh\psi_0 + \sin(\beta\mp\gamma)}{\cos\beta\tanh\psi_0 + \cos(\beta\mp\gamma)},$$
$$\tan t_{1,2} = \frac{\sin\beta + \tanh\psi_0\sin(\beta\mp\gamma)}{\cos\beta + \tanh\psi_0\cos(\beta\mp\gamma)},$$

where ϕ_1 corresponds to the plus sign in $\beta\mp\gamma$ and ϕ_2 corresponds to the minus sign. The components of the shift vector (ϕ_0,τ_0) are

$$\phi_0 = \phi_1 - \phi_2, \qquad \tau_0 = \tau_1 - \tau_2$$

and can be written as

$$\tau_0 = -2\arctan\frac{\tanh\psi_0\sin\gamma}{1+\tanh\psi_0\cos\gamma}, \qquad \phi_0 = -2\arctan\frac{\sin\gamma}{\tanh\psi_0+\cos\gamma}, \tag{15}$$

which agrees with the result in [15] up to a sign.

2.3. Geodesic approximation in AdS/CFT. To clarify a holographic interpretation of the construction described above, we step aside and discuss another topic: the geodesic approximation in holography. A basic element in the AdS/CFT dictionary is the correspondence between the conformal dimensions of operators in the boundary field theory and the masses of dual fields in the bulk. More concretely, if we consider a boson or fermion field of mass $m_{\text{b,f}}$ in the AdS bulk and the AdS radius is set equal to L, then we have the respective relations

$$\Delta_{\text{b}} = \frac{d}{2} + \frac{1}{2}\sqrt{d^2 + 4m_{\text{b}}^2L^2} \qquad \text{and} \qquad \Delta_{\text{f}} = \frac{1}{2} + m_{\text{f}}L$$

for bosons and fermions, where d is the number of boundary dimensions. In this case, $d = 2$.

If the bulk field mass is very high, $mL \gg 1$, then it is natural to expect that the bulk excitation would move along a classical trajectory with a low probability of substantial deviations from it. Therefore, the semiclassical approximation of geometric optics is applicable, and we can assume that all information relevant for two-point correlation functions is encoded in the lengths of classical geodesics connecting boundary points.

The geodesic approximation is a very simple and effective tool for analyzing the boundary theory [8]. To begin with, we consider the case of an empty AdS_3 space. We work with global coordinates (1). The conformal boundary is set as $\chi\to\infty$ or $r\to 1$ in notation (2).

For equal time geodesics (for $d\tau = 0$), we have $dL^2 = d\chi^2 + \sinh^2\chi\, d\phi^2$. Because the space–time metric diverges near the boundary, the geodesic lengths of interest are formally infinite and must therefore be renormalized (we let L_{ren} denote the renormalized geodesic length). The simplest way to renormalize is to introduce an ultraviolet cutoff taking geodesics between two points with the (χ,ϕ) coordinates $(\chi_{\text{m}},-\phi_{\text{m}})$ and $(\chi_{\text{m}},\phi_{\text{m}})$. It is easy to see that the length of such a geodesic is (cf. [16])

$$L = \log\frac{4\sin^2\phi_{\text{m}}}{\delta^2},$$

where $\delta \approx 2e^{-\chi_m}$ is a regularization parameter. The natural answer for the renormalized length in this case is

$$L_{\text{ren}} = \log(4\sin^2\phi_m).$$

From the invariance under rotation in ϕ, we have

$$L_{\text{ren}}((0,\phi_1);(0,\phi_2)) = \log\left(4\sin^2\frac{\phi_1-\phi_2}{2}\right).$$

Hence, for the two-point correlation function, we finally obtain

$$\langle \mathcal{O}_\Delta(0,\phi_1)\mathcal{O}_\Delta(0,\phi_2)\rangle = e^{-\Delta L_{\text{ren}}} = \left(\frac{1}{4\sin^2((\phi_1-\phi_2)/2)}\right)^\Delta.$$

We see that we have singularities at $\phi_1-\phi_2 = 2\pi n$. Generalizing this expression to the case of an arbitrary metric and non-equal-time geodesics, we obtain

$$\langle \mathcal{O}_\Delta(t_1,x_1)\mathcal{O}_\Delta(t_2,x_2)\rangle = e^{-\Delta L_{\text{ren}}(t_1,x_1;t_2,x_2)} \tag{16}$$

for the two-point correlation function of operators of conformal weight $\Delta \gg 1$.

If the two points are separated by a timelike interval, $(t_1-t_2)^2 > (\phi_1-\phi_2)^2$, then a certain subtlety arises in using this prescription. In that case, there is no real geodesic connecting such points. But we can obtain an answer for the correlation function by introducing the notion of complexified geodesics similarly to how this was done for the Poincaré disk [17] (see the appendix for details). Holographic relation (16) remains unchanged, and the renormalized two-point correlation function in the AdS_3 space becomes

$$\langle \mathcal{O}_\Delta(\tau_1,\phi_1)\mathcal{O}_\Delta(\tau_2,\phi_2)\rangle = e^{-\Delta L_{\text{ren}}} = \left(\frac{1}{\cos(\tau_1-\tau_2)-\cos(\phi_1-\phi_2)}\right)^\Delta. \tag{17}$$

3. The Green's function in the coordinate representation

3.1. Stationary conical defect. Speaking in terms of the geodesic approximation, it is very easy to understand how the presence of a conical defect changes the properties of the boundary field theory. Before, we had a single geodesic (real or complex) connecting a given pair of points in the empty AdS_3 space. Placing a conical defect in the bulk leads to lensing of geodesics in the sense that a pair of points can now be connected by several geodesics winding around the conical singularity.

Identity (16) then becomes

$$\langle \mathcal{O}_\Delta(t_1,x_1)\mathcal{O}_\Delta(t_2,x_2)\rangle = \sum_{i=1}^{n} e^{-\Delta L^i_{\text{ren}}(t_1,x_1;t_2,x_2)}$$

(here the index i labels all possible geodesics connecting the given points). If we take into account that the contribution of nonminimal geodesics is damped for large Δ, then we have

$$\langle \mathcal{O}_\Delta(t_1,x_1)\mathcal{O}_\Delta(t_2,x_2)\rangle \simeq \max_{i=1,\dots,n} e^{-\Delta L^i_{\text{ren}}(t_1,x_1;t_2,x_2)}.$$

We use the first formula to calculate correlation functions, because it allows smoothing unphysical singularities that arise when two geodesics l_1 and l_2 connecting the points (t_1,x_1) and (t_2,x_2) have the same length. Moreover, despite the smallness of contributions from nonminimal geodesics, precisely they can lead

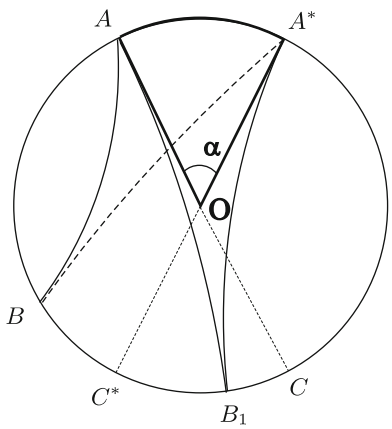

Fig. 1. The deficit angle $2\gamma < \pi$: for $|\phi_A - \phi_B| < \pi - 2\gamma$, there is only one geodesic AB connecting the identified points A and A^* on the boundary of the removed wedge with the point B (shown by the solid line; the dashed line A^*B is not physically real). For a point B_1 between C and C^*, i.e., such that $|\phi_A - \phi_B| > \pi - 2\gamma$, there are two physically different geodesics AB_1 and A^*B_1 connecting the point B_1 with A and A^*.

to physically nontrivial effects in certain situations (this is especially obvious in the case of two rotating conical defects, which we consider in a separate paper).

As stated above, the deformed space arising when a massive source is placed in the bulk AdS_3 space can be represented as a cone, a space with an excised wedge and identified faces. This approach to visualization should be used with care: it should rather be said that space–time is squeezed in a certain way to become a cone, and no physical points are actually removed in this procedure.

The metric structure of the space–time is unchanged locally, which allows representing geodesics on the cone in terms of their corresponding geodesics in the empty AdS_3 space. It is easiest to understand the geodesic structure of such a cone by looking at Figs. 1 and 2. For now, we speak about geodesics in a constant-time section for simplicity.

We first discuss the case where the deficit angle is $2\gamma < \pi$. The points A and A^* belonging to identified faces of the wedge are physically equivalent. An arbitrary boundary point B satisfying the condition $|\phi_A - \phi_B| < \pi - 2\gamma$ can be connected with each of them by not more than one geodesic (connected by two geodesics if $\pi - 2\gamma < |\phi_A - \phi_B| < \pi$; see Fig. 1). The total number of geodesics in this case is either one or two, and the corresponding correlation function up to normalization is given by

$$\langle \mathcal{O}_\Delta(A)\mathcal{O}_\Delta(B)\rangle = e^{-\Delta L_{\rm ren}(B;A)}\theta(\pi - (\phi_B - \phi_A)) + e^{-\Delta L_{\rm ren}(B;A^*)}\theta(\pi - (\phi_B - \phi_A^*)) =$$

$$= \frac{\theta(\pi - (\phi_B - \phi_A))}{(\cos(\phi_A - \phi_B))^\Delta} + \frac{\theta(\pi - (\phi_B - \phi_A^*))}{(\cos(\phi_A^* - \phi_B))^\Delta}.$$

If $\pi < 2\gamma < 2\pi$ (see Fig. 2), then physically distinct points A and B can be connected by a finite number of geodesics (now at least two). This is easily seen if we cover the Poincaré disk with an atlas whose charts are unfolded cones (i.e., sectors of a circle with the angle $\pi - 2\gamma$). In such a representation, the point A has a number of images on the Poincaré disk in addition to A^* (points A_1 and A_2 in Fig. 2), and each geodesic connecting B with one of these images can be folded back onto the physical conical space connecting B with A or A^* but now winding around the conical singularity.

If the deficit angle is such that $2\pi - 2\gamma = 2\pi/n + \alpha$, where $0 < \alpha < 2\pi/n$, then the maximum number of

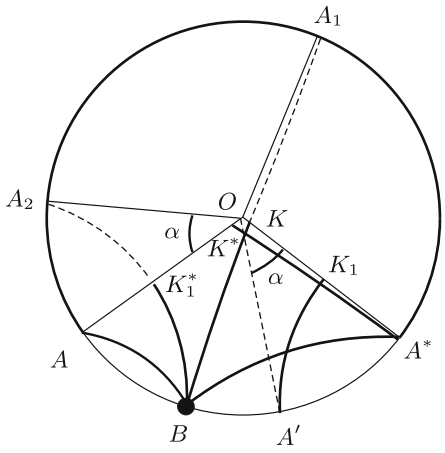

Fig. 2. The cone angle is not equal to $2\pi/n$, $n \in \mathbb{N}$. We show the case $2\pi - 2\gamma = 2\pi/3 + \alpha$, where $\alpha < 2\pi/3$ (here $n = 3$). The geodesics AB and A^*B are in the physical sector AOA^*. The geodesic BA_1 leaves the physical sector; its part KA_1 (shown by a dashed line) is outside the physical sector. The part A_1K under rotation of the disk through the angle $2\pi - 2\gamma$ passes into the part of the geodesic A^*K^*, and the length of the geodesic A_1B is the sum of the lengths of the parts KB and A^*K^*. The line BA_1 can be represented as the result of winding around the conical singularity. The winding consists of KB and A^*K^*. The geodesic A_2B leaving the physical sector can be represented as the winding consisting of K_1^*B and $A'K_1$.

geodesics can be equal to $w_{\max} = n$ (see Fig. 2), and the Green's function of the boundary theory becomes

$$\langle \mathcal{O}_\Delta(A)\mathcal{O}_\Delta(B)\rangle \sim \sum_{l=0}^{\cdots} \frac{\theta(\pi - |\phi_B - \phi_A - 2l(\pi-\gamma)|)}{|\cos(\phi_B - \phi_A - 2l(\pi-\gamma))|^\Delta} + \sum_{l=0}^{\cdots} \frac{\theta(\pi - |-\phi_B + \phi_A^* + 2l(\pi-\gamma)|)}{|\cos(\phi_A^* + 2l((\pi-\gamma) - \phi_B)|^\Delta},$$

where the ellipsis in the upper limit of the sums means that we should sum until the Heaviside function becomes zero.

If the deficit angle is such that $2\pi - 2\gamma = 2\pi/n$, $n \in \mathbb{N}$, then n terms contribute to the correlation functions (see Fig. 3), and the Green's function becomes

$$\langle \mathcal{O}_\Delta(A)\mathcal{O}_\Delta(B)\rangle \sim \sum_{l=0}^{n-1} \frac{1}{|\cos(\phi_B - \phi_A - 2l(\pi-\gamma))|^\Delta}.$$

To generalize this reasoning to the case of arbitrary geodesics (not only those in a constant-time section), we must use the algebraic representation described in Sec. 2.1.

Obviously, the main contribution to correlation functions is from the geodesics that do not wind around the conical singularity. As an example, we show correlation functions for operators of zero conformal weight in Fig. 4.[2] In Fig. 4a, we show the graph of the correlation function $-\log[(1-\cos\phi)/2]$, $0 < \phi < 2\pi$. In Fig. 4b, we compare the contribution to the correlation function $-\log[(1-\cos\phi)/2]$ (thick line) and the contribution $-\log[(1-\cos(\phi-1.9\pi))/2]$, i.e., corresponding to a small deficit angle (thin line), for $0 < \phi < \pi$. In Fig. 4c, we show the Green's function given at each point as the maximum of the two contributions in

[2]Of course, the geodesic approximation formally holds for $\Delta \gg 1$, and $\Delta = 0$ is far beyond its applicability region. Nevertheless, we can still hope that the geodesic approximation allows obtaining qualitatively true results.

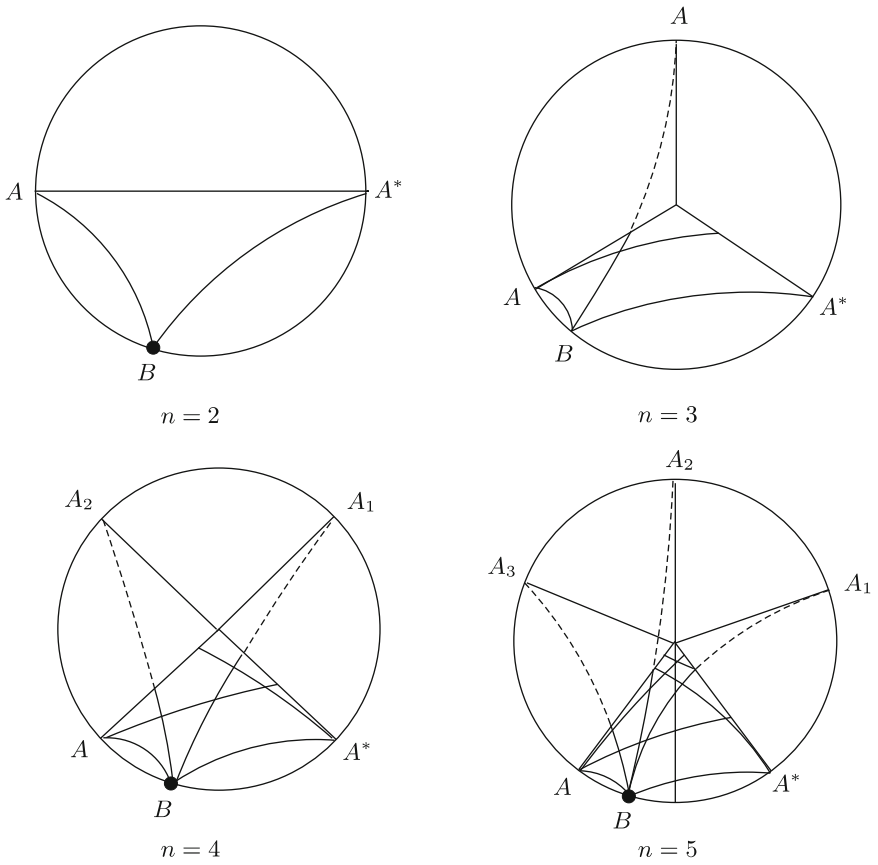

Fig. 3. The cone angle is an integer part of 2π, i.e., the deficit angle 2γ satisfies the relation $2\pi - 2\gamma = 2\pi/n$ with $n = 2, 3, 4, 5$.

Fig. 4b for $0 < \phi < \pi$. In Fig. 4d, the thick line represents the contribution to the correlation function $-\log[(1-\cos\phi)/2]$, and the thin line represents the contribution to $-\log[(1-\cos(\phi-\pi))/2]$, $0 < \phi < 2\pi$. In Fig. 4e, we show the Green's function given as the maximum of the two contributions in Fig. 4d for $0 < \phi < \pi$. In Fig. 4f, the thick, thin, dashed, and dash-dotted lines are the respective contributions to the correlation functions $-\log(1-\cos\phi)/2$, $-\log[(1-\cos(\phi-0.4\pi))/2]$, $-\log[(1-\cos(\phi-2\cdot 0.4\pi))/2]$, and $-\log[(1-\cos(\phi-3\cdot 0.4\pi))/2]$ for $0 < \phi < 2\pi$. In Fig. 4g, we show the Green's function given as the maximum of the four contributions in Fig. 4f for $0 < \phi < 0.4\pi$.

3.2. Comparison of one- and two-geodesic approximations. As mentioned above, the one-geodesic approximation works well for large conformal weights Δ. But taking only the shortest geodesic into account leads to kinks in the correlation function at the points of "geodesic change" (see Fig. 5). We can eliminate these singularities if we take the next-to-leading geodesic into account and add it to the leading contribution.

A similar picture also holds for unequal-time geodesics. We consider the Euclidean version of unequal-time correlation functions for operators of conformal weight $\Delta = 0$. We show the calculation results in Fig. 6. Correlation functions in the space of a moving particle contain more singularities.

3.3. Moving conical defect. In this section, we consider correlation functions of the theory on the boundary of the AdS_3 space with one massive pointlike particle moving along the spiral

$$\langle \mathcal{O}_\Delta(A)\mathcal{O}_\Delta(B)\rangle_{\mathrm{MP}} \equiv G_\Delta(\tau,\phi|\tau_0,\phi_0),$$

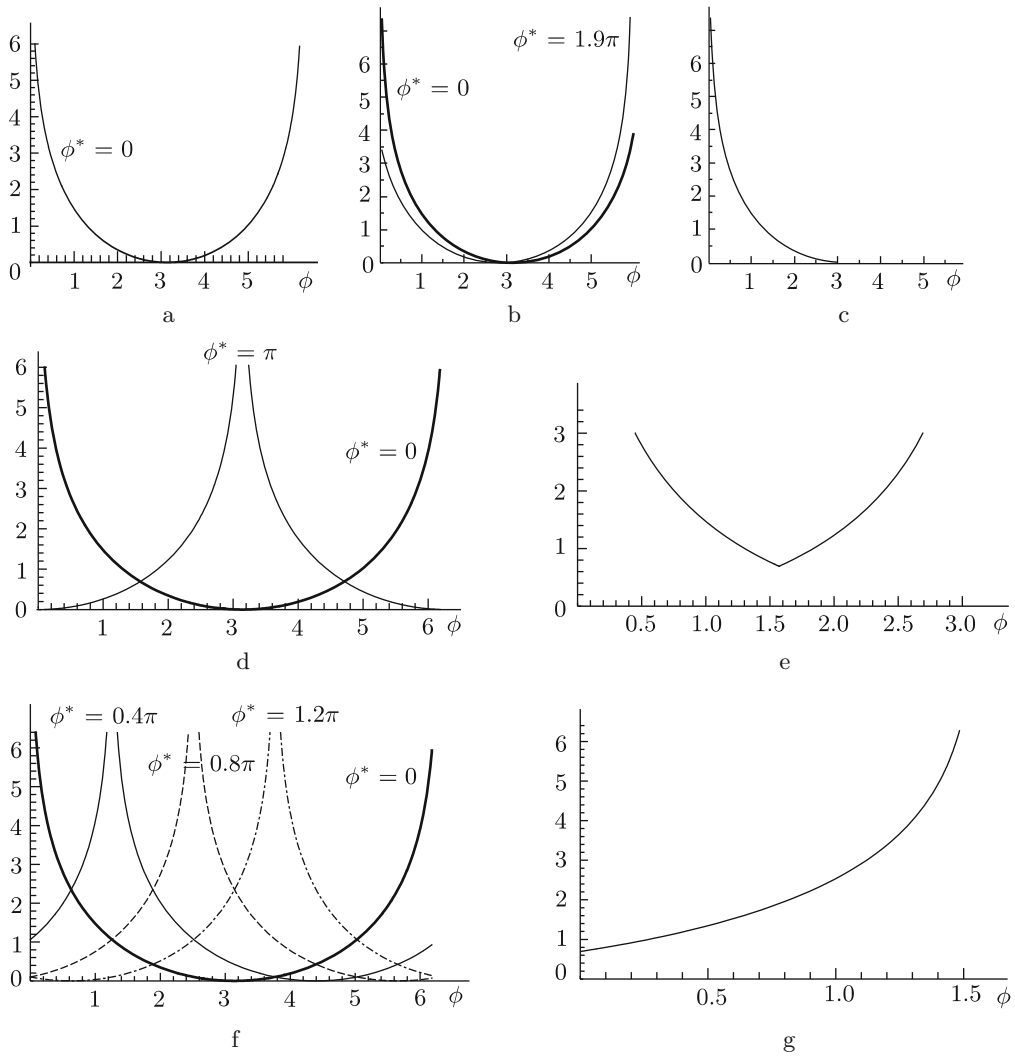

Fig. 4. Contributions to the equal-time correlation functions of the form $-\log\big(\big(1-\cos(\phi-\phi^*)\big)/2\big)$, $0 < \phi < 2\pi$, related to different geodesics (for different values of ϕ^*): plots (c), (e), and (g) show functions given as the maximum of the functions in the respective neighboring plots (b), (d), and (f) (on a smaller interval of the values ϕ).

where $A = (0,0)$, $B = (\tau,\phi)$, and the identification vector (τ_0,ϕ_0) is determined by the moving particle.

In the one-geodesic approximation, the function $G_\Delta(\tau,\phi|\tau_0,\phi_0)$ is given by

$$G_\Delta(\tau,\phi|\tau_0,\phi_0) = \frac{\theta(-|\cos\tau-\cos\phi| + |\cos(\tau-\tau_0)-\cos(\phi-\phi_0)|)}{(\cos\tau-\cos\phi)^\Delta} + \\ + \frac{\theta(|\cos\tau-\cos\phi| - |\cos(\tau-\tau_0)-\cos(\phi-\phi_0)|)}{(\cos(\tau-\tau_0)-\cos(\phi-\phi_0))^\Delta}. \tag{18}$$

For the moving particle, the components of the identification vector (τ_0,ϕ_0) are determined by the particle kinetics. The position of the image point corresponding to this vector is shown in Fig. 7.

To analyze the properties of function (18), we consider the inverse propagator of the field of conformal

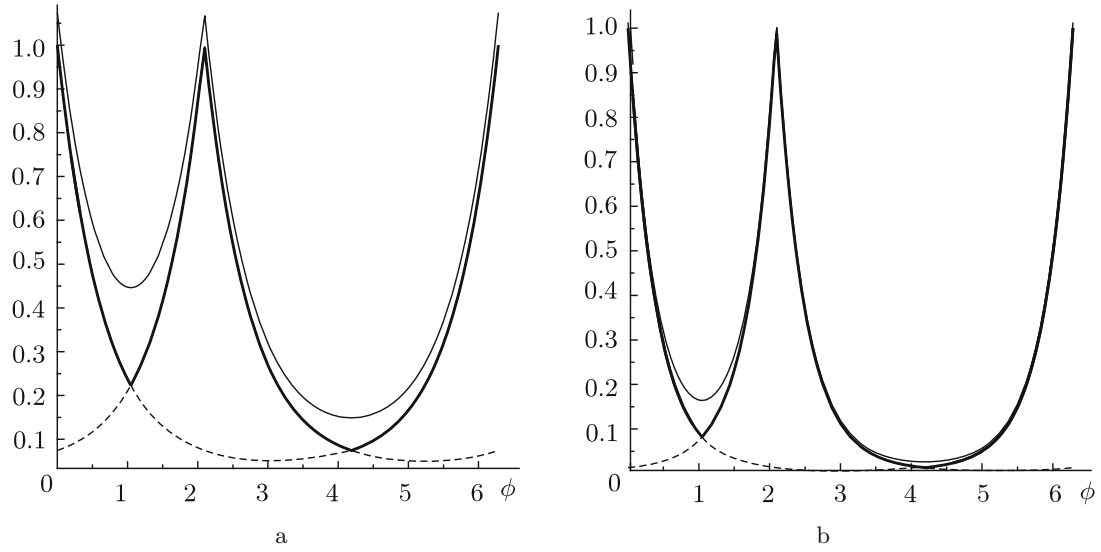

Fig. 5. (a) The contribution of the shortest geodesic to the equal-time correlation function for the conformal weight $\Delta = 1$ is shown by the thick line; the two-geodesic approximation is shown by the thin line. (b) The same picture for $\Delta = 3$.

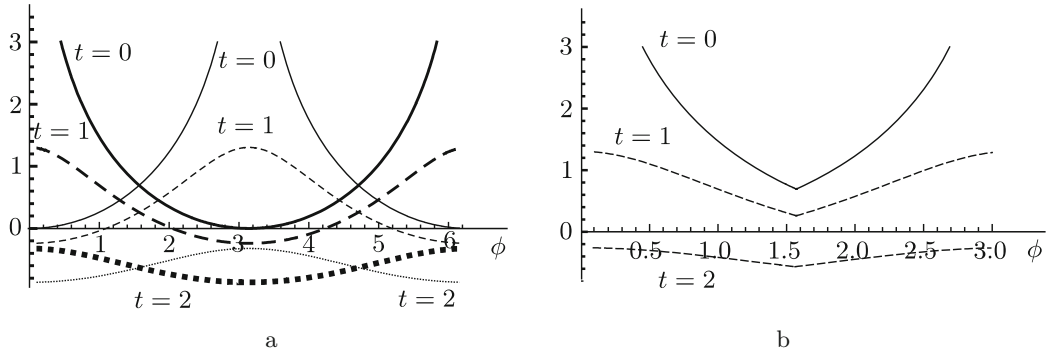

Fig. 6. (a) Correlation functions $-\log[(\cosh t - \cos\phi)/2]$ (shown with thick lines) and $-\log[(\cosh t - \cos(\phi - \pi))/2]$ (thin lines) for different t. (b) Correlation functions defined as the maximum of two corresponding correlation functions (shown by the same type of thick and thin lines) in picture (a) for $0 < \phi < \pi/2$.

weight $\Delta = 1$ for different identification vectors:

$$F(\tau,\phi) = f_1(\tau,\phi)\theta(-|\cos\tau - \cos\phi| + |\cos(\tau-\tau_0) - \cos(\phi-\phi_0)|) + \\ + f_2(\tau,\phi)\theta(|\cos\tau - \cos\phi| - |\cos(\tau-\tau_0) - \cos(\phi-\phi_0)|), \tag{19}$$

$$f_1(\tau,\phi) = \cos\tau - \cos\phi, \qquad f_2(\tau,\phi) = f(\tau-\tau_0, \phi-\phi_0).$$

The function $F(\tau,\phi)$ has zeros (poles of the function $G_\Delta(\tau,\phi|\tau_0,\phi_0)$), jumps, and kinks. The zeros are at the points where at least one of the functions $f_1(\tau,\phi)$ or $f_2(\tau,\phi)$ is zero. The zeros of $f(\tau,\phi)$ correspond to positions of generatrices of the original light cone in the boundary field theory; the zeros of $f_2(\tau,\phi)$ are

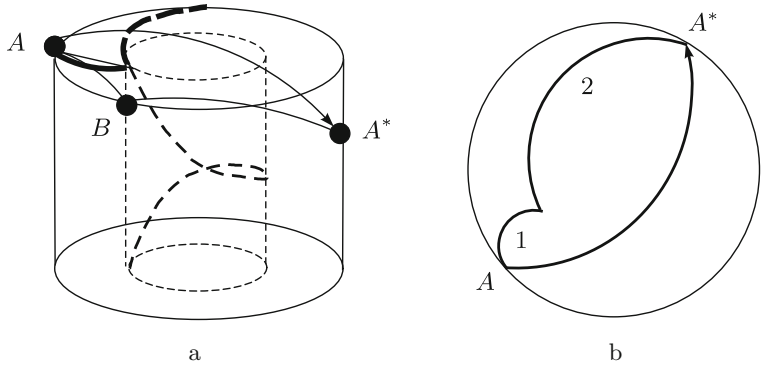

Fig. 7. (a) A schematic three-dimensional picture of the AdS_3 space with a massive particle moving along a spiral (its trajectory is shown by the thick dashed line): the deficit angle is less than π; the arrow from A to A^* shows the identified points A and its image A^*. (b) A section for a constant time coordinate τ of the conical AdS_3 space: the thick lines denote the identified wedge faces; the points A and A^* belong to different constant-time sections.

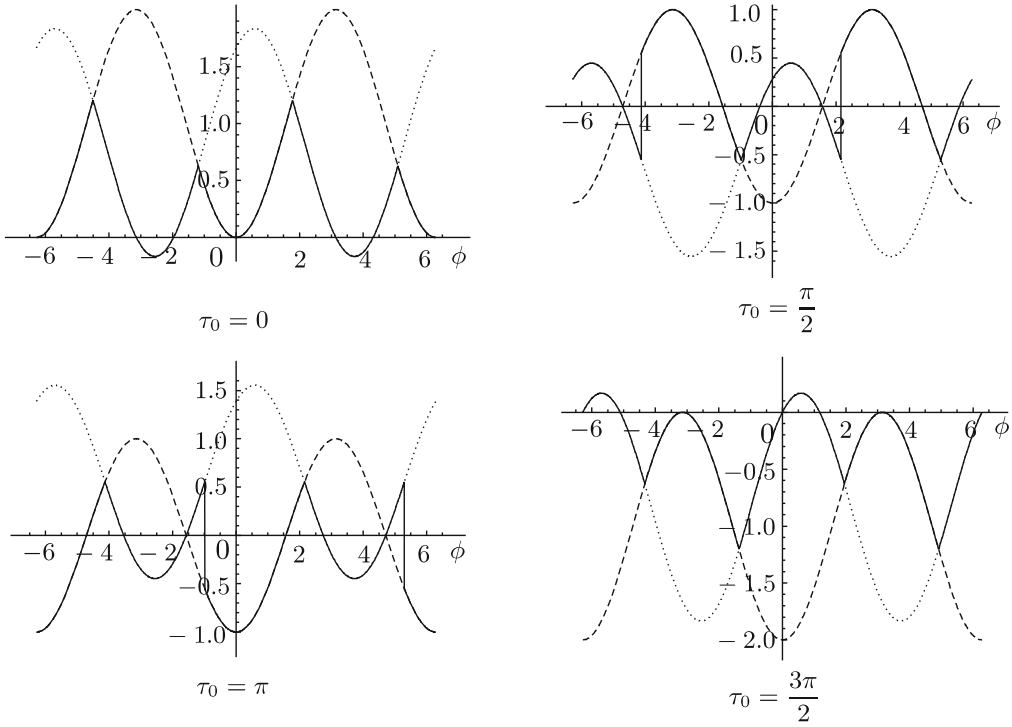

Fig. 8. The functions $f_1(\tau, \phi)$ (dashed lines), $f_2(\tau, \phi)$ (dotted lines), and $F(\tau, \phi)$ (solid lines) given by (19) for $\phi_0 = \pi/2$ and different values of τ_0.

shifted to (τ_0, ϕ_0) because of the lensing effect. There are also jumps at

$$|\cos\tau - \cos\phi| = |\cos(\tau - \tau_0) - \cos(\phi - \phi_0)|, \qquad \cos\tau - \cos\phi \neq \cos(\tau - \tau_0) - \cos(\phi - \phi_0)$$

and kinks at

$$\cos\tau - \cos\phi = \cos(\tau - \tau_0) - \cos(\phi - \phi_0), \qquad \cos\tau - \cos\phi \neq 0.$$

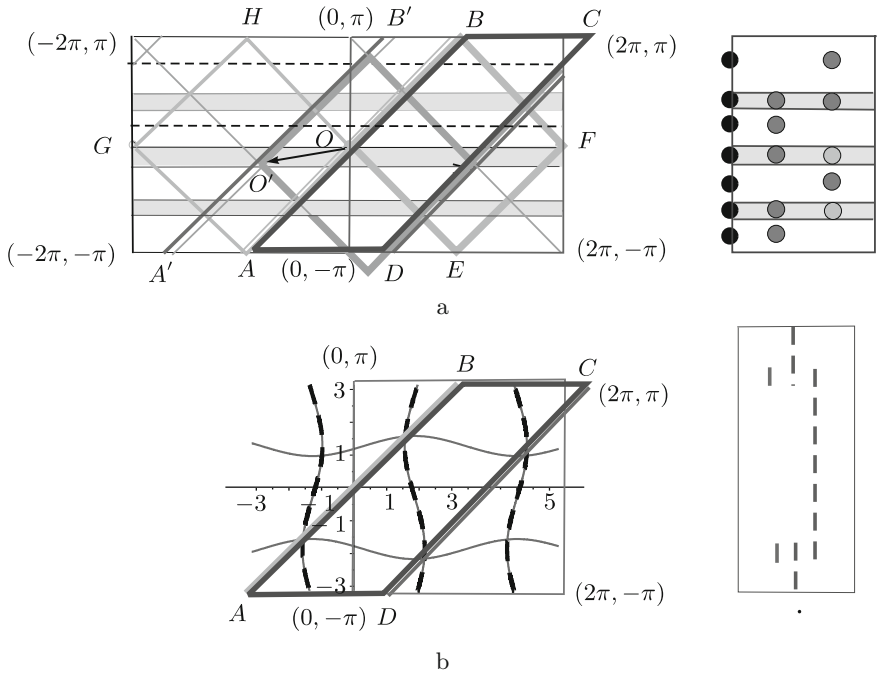

Fig. 9. (a) The causal structure of the space–time containing a moving conical defect (left) and the corresponding propagator strips in the physical space (right). (b) The movement of the skips (solid lines) and jumps (dashed lines) of the generator of the Green's function (left) and also the appearance and disappearance in time of the skips and jumps (right).

For the shortest-geodesic approximation and the two-geodesic approximation, we respectively have

$$G^{(1)}_{\Delta}(\tau,\phi) = \frac{\theta(-|\cos\tau-\cos\phi|+|\cos(\tau-\tau_0)-\cos(\phi-\phi_0)|)}{(\cos\tau-\cos\phi)^{\Delta}} + \\ + \frac{\theta(|cos\tau-\cos\phi|-|\cos(\tau-\tau_0)-\cos(\phi-\phi_0)|)}{(\cos(\tau-\tau_0)-\cos(\phi-\phi_0))^{\Delta}},$$

$$G^{(2)}_{\Delta}(\tau,\phi) = \frac{1}{(\cos\tau-\cos\phi)} + \frac{1}{(\cos(\tau-\tau_0)-\cos(\phi-\phi_0))^{\Delta}}.$$

Compared with $G^{(2)}_{\Delta}(\tau,\phi)$, $G^{(1)}_{\Delta}(\tau,\phi)$ has jumps (see Fig. 8).

We consider the case where the identification vector has two independent components (τ_0,ϕ_0). The movements of kinks and jumps are shown in Fig. 9.

In fig. 9a, we show the causal structure of the space–time containing a moving conical defect (left) and the corresponding propagator strips in the physical space (right). The deficit angle is less than π. The lines AB and $A'B'$ are identified, and the identification vector is shown by the arrow OO'. The rectangle with the vertices $(-2\pi,-\pi)$, $(-2\pi,\pi)$, $(2\pi,\pi)$, and $(2\pi,\pi)$ corresponds to the boundary of the original cylinder. The parallelogram $ABCD$ bounds the area remaining after the cut-and-glue procedure. The squares $OBFE$ and $OAGH$ show the causal structure of the light cones in the original undeformed field theory (they denote the poles of the Green's function with $\tau_0=0$ and $\phi_0=0$). The shifted square with vertices at the points D and O' demonstrate the additional poles of the Green's function appearing as a result of the gravitational lensing effect. In the picture on the right, the number of dark "abacus beads" is equal to the number of basic poles of the propagator in the physical space, and the pale "beads" correspond to the additional poles that arise from the lensing.

In the picture on the left in Fig. 9b, the wavy solid and dashed lines show the movement of the corresponding skips and jumps of the generator of the Green's function, and the appearance and disappearance in time of the skips (solid lines) and jumps (dashed lines) of the generator are shown schematically in the picture on the right.

4. The Green's function in the momentum representation

4.1. Quantized stationary conical defects. To consider the momentum representation of correlation functions (18), it is convenient to perform the Wick rotation $\tau \to \tau_{\text{E}} = i\tau$ first,

$$\mathcal{G}_\Delta(\tau_{\text{E}},\phi|\tau_{0\text{E}},\phi_0) = \frac{\theta(-|\cosh\tau_{\text{E}} - \cos\phi| + |\cosh(\tau_{\text{E}} - \tau_{0E}) - \cos(\phi-\phi_0)|)}{(\cosh\tau_{\text{E}} - \cos\phi)^\Delta} + \\ + \frac{\theta(|\cosh\tau_{\text{E}} - \cos\phi| - |\cosh(\tau_{\text{E}} - \tau_{0E}) - \cos(\phi-\phi_0)|)}{(\cosh(\tau_{\text{E}} - \tau_{0\text{E}}) - \cos(\phi-\phi_0))^\Delta}, \tag{20}$$

and then take the Fourier transform. We note that the Euclidian correlation function with $\Delta = 0$ is related to the Green's function of the Laplace operator on a cylinder,

$$\mathcal{G}_0(\tau_{\text{E}},\phi) = \log(2(\cosh\tau_{\text{E}} - \cos\phi)). \tag{21}$$

This correlation function can be obtained from the expression for the correlation function of weight $\Delta = 0$ on the plane

$$\langle\Phi_0(z_1,\bar z_1)\Phi_0(z_2,\bar z_2)\rangle = \log(|z_1 - z_2|^2)$$

via the conformal map $w = \log z$ from the two-dimensional plane to the cylinder:

$$\langle\Phi_0(w_1,\bar w_1)\Phi_0(w_2,\bar w_2)\rangle = -\log\left(4\sinh\frac{w_1-w_2}{2}\sinh\frac{\bar w_1 - \bar w_2}{2}\right).$$

Introducing the notation

$$w = w_1 - w_2 = \tau_{\text{E}} + i\phi, \qquad \bar w = \bar w_1 - \bar w_2 = \tau_{\text{E}} - i\phi,$$

we obtain (21).

We note that by virtue of the relation[3]

$$\sum_{\substack{-\infty\le n\le\infty,\\ n\ne 0}} \int_{-\infty}^{\infty} \frac{e^{ip\tau_{\text{E}}+iq\phi}}{p^2+n^2}dp = \pi\tau_{\text{E}} - \pi\log\left(4\sinh\frac{\tau_{\text{E}}-i\phi}{2}\sinh\frac{\tau_{\text{E}}+i\phi}{2})\right), \quad \tau_{\text{E}} > 0,$$

we have the standard momentum representation with the continuous 0-component p and discrete 1-component r of the momentum:

$$\int_0^{2\pi}\frac{d\phi}{2\pi}\int_{-\infty}^{\infty}\frac{dt}{2\pi}e^{-itp-i\phi r}\langle\Phi_0(t,\phi)\Phi_0(0,0)\rangle = \\ = -\int_0^{2\pi}\frac{d\phi}{2}\int_{-\infty}^{\infty}\frac{dt}{2\pi}e^{-itp-i\phi r}\log(1-e^{-|t|+i\phi})(1-e^{-|t|-i\phi}) = \frac{1}{p^2+r^2}. \tag{22}$$

[3]Here, we subtract the contribution from the null harmonic $n = 0$ to avoid problems with the infrared divergence.

Below, we find the analogue of representation (22) for the correlation function in the field theory dual to the AdS_3 space–time with a stationary massive particle at the center of the Poincaré disk. We have

$$\mathcal{G}_{\text{1-c}}\left(p, \frac{2\pi}{L_0}r\right) = \int_0^{L_0} \frac{d\phi}{L_0} \int_{-\infty}^{\infty} \frac{dt}{2\pi} e^{-itp - i\phi(2\pi/L_0)r} \langle \Phi_0(t,\phi)\Phi_0(0,0)\rangle_{\text{1-c}},$$

where $L_0 = 2\pi - 2\gamma$ and

$$\langle \Phi_0(t,\phi)\Phi_0(0,0)\rangle_{\text{1-c}} = \langle \Phi_0(t,\phi)\Phi_0(0,0)\rangle\, \theta\left(\frac{L_0}{2} - \phi\right) + \langle \Phi_0(0,L_0)\Phi_0(t,\phi)\rangle\, \theta\left(\phi - \frac{L_0}{2}\right).$$

Here, $\langle \Phi_0(t,\phi)\Phi_0(0,0)\rangle$ is given by (20). Therefore,

$$\begin{aligned}\mathcal{G}_{\text{1-c}}\left(p, \frac{2\pi}{L_0}r\right) = &-\int_0^{L_0/2} \frac{d\phi}{2L_0} \int_{-\infty}^{\infty} dt\, e^{-itp - i\phi(2\pi/L_0)r} \log(1 - e^{-|t| + i\phi\cdot 2\pi/L})(1 - e^{-|t| - i\phi}) - \\ &- \int_{L_0/2}^{L_0} \frac{d\phi}{2L_0} \int_{-\infty}^{\infty} dt\, e^{-itp - i\phi(2\pi/L_0)r} \log(1 - e^{-|t| + i(L_0 - \phi)})(1 - e^{-|t| - i(L_0-\phi)}). \end{aligned} \tag{23}$$

To calculate this integral, we integrate by parts and represent $\mathcal{G}_{\text{1-c}}$ as a sum:

$$\mathcal{G}_{\text{1-c}}\left(p, \frac{2\pi}{L_0}r\right) = B_1 + M_1 + N_1 + B_2 + M_2 + N_2,$$

where

$$\begin{aligned} M_1 &= \int_0^{L_0/2} d\phi\, \frac{e^{-i\phi(2\pi/L_0)r}}{2r} \int_{-\infty}^{\infty} \frac{dt}{2\pi} e^{-itp} \frac{e^{-(2\pi/L_0)|t| + i}}{1 - e^{-|t| + i\phi}}, \\ M_2 &= -\int_{L_0/2}^{L_0} d\phi\, \frac{e^{-i\phi(2\pi/L_0)r}}{2r} \int_{-\infty}^{\infty} \frac{dt}{2\pi}\, e^{-itp} \frac{e^{-iL_0} e^{-|t| - i\phi}}{1 - e^{-iL_0} e^{-|t| - i\phi}}, \end{aligned}$$

N_1 and N_2 correspond to contributions of the second factor in the right-hand side of (23), and B_1 and B_2 are the boundary terms,

$$\begin{aligned} B_1 = &\frac{e^{-i\pi r}}{2ir} \int_{-\infty}^{\infty} \frac{dt}{2\pi} e^{-itp} \log((1 - e^{-|t| + i\pi L_0/L})(1 - e^{-|t| - i\pi L_0/L})) - \\ &- \frac{1}{2ir} \int_{-\infty}^{\infty} \frac{dt}{2\pi} e^{-itp} \log((1 - e^{-|t|})(1 - e^{-|t|})), \\ B_2 = &\frac{e^{-2i\pi r}}{2ir} \int_{-\infty}^{\infty} \frac{dt}{2\pi} e^{-itp} \log((1 - e^{-iL_0} e^{-|t| - 2i\pi L_0/L})(1 - e^{iL_0} e^{-|t| + 2i\pi L_0/L})) - \\ &- \frac{e^{-i\pi r}}{ir} \int_{-\infty}^{\infty} \frac{dt}{2\pi} e^{-itp} \log((1 - e^{-iL_0} e^{-|t| - i\pi L_0/L})(1 - e^{iL_0} e^{-|t| + i\pi L_0/L})). \end{aligned}$$

Expanding the denominators in the expressions for M_i, we obtain

$$M_1 = \frac{1}{2} \sum_{k=1}^{\infty} \int_0^{L_0/2} d\phi\, \frac{e^{-i\phi(2\pi/L_0)r}}{r} \int_{-\infty}^{\infty} \frac{dt}{2\pi} e^{-itp} e^{-(2\pi k|t|/L + i\phi k)}.$$

Integrating over t and ϕ, we obtain an explicit representation for M_1 in the form of a series. Similar expressions hold for M_2 and N_i. As a result, we have

$$M_1 + M_2 + N_1 + N_2 = \frac{1}{2\pi r}\sum_{k=1}^{\infty}\frac{k\,F(k,r,L_0)}{p^2+k^2},$$

where

$$F(k,r,L_0) = i\frac{e^{-i(\pi r - kL_0/2)} + e^{-i(2\pi r - 2kL_0)} - e^{-i(\pi r - 3kL_0/2)} - 1}{2\pi r/L_0 - k} -$$
$$- i\frac{e^{-i(\pi r + kL_0/2)} + e^{-i(2\pi r + 2kL_0)} - e^{-i(\pi r + 3kL_0/2)} - 1}{2\pi r/L_0 + k}.$$

We consider the case $L_0 = \pi$. For integer r, we have

$$\operatorname{Im} F(k,r,\pi) = \frac{2\sin(k\pi/2)[\sin(k\pi/2) + \sin(3k\pi/2)]}{k^2 - 4r^2},$$

$$\operatorname{Re} F(k,r,2\pi,\pi) = \frac{4r\sin(k\pi/2)[\cos(k\pi/2) + \cos(3k\pi/2) - \cos(\pi k)\cos(\pi r)]}{k^2 - 4r^2}.$$

Therefore, $\operatorname{Im} F(k,r,\pi) = 0$ for any integer k, while $\operatorname{Re} F(k,r,\pi) = 0$ only for even k. We can also verify that the identity $B_1 + B_2 = 0$ holds for $L_0 = \pi$.

For the correlation functions, we finally obtain

$$\mathcal{G}_{1\text{-c}}(p,r,\pi) = \frac{1}{\pi}\sum_{n=1}^{\infty}\frac{(2n+1)(-1)^n}{p^2+(2n+1)^2}\frac{(-1)^r}{(2n+1)^2 - 4r^2}.$$

After the Wick rotation, we have

$$G_{1\text{-c}}(E,r,\pi) = \frac{1}{\pi}\sum_{n=1}^{\infty}\frac{2n+1}{(2n+1)^2 - E^2}\frac{(-1)^{r+n}}{(2n+1)^2 - 4r^2}. \tag{24}$$

It is easy to see that these functions have poles at integer values of the energy E and the residues are real but can be both positive and negative. A remarkable fact is that the 0- and 1-components of the momentum are absolutely independent of each other, and the notion of a dispersion relation is undefined in such a theory. Apparently, result (24) can be interpreted as a sum of contributions of homogeneously "distributed" excitations of the domain wall type on half of the cylinder (as we understand, the physical space of the theory in the cut-and-glue representation is half of the cylinder).

It would be interesting to know whether these excitations are real physical objects or merely artifacts of the one-geodesic approximation, disappearing when higher corrections are taken into account.

4.2. Euclidean version of correlation functions with a nontrivial identification vector (τ_0, ϕ_0). Before analyzing the correlation functions corresponding to a moving particle, we consider the Euclidean version of correlation functions with an arbitrary identification vector (see Fig. 10). In Fig. 10a, we show the dependence of the real (solid line) and imaginary (dashed line) parts of the correlation function in the momentum representation on the discrete 1-component r of the momentum. It can be seen that the imaginary part is zero at integer points. In Fig. 10b, we show the dependence of the real part of the correlation function on the deficit angle γ at the integer value $r = 2$. In Fig. 10c, we show the dependence of the real part of the correlation function in the momentum representation on the continuous 0-component

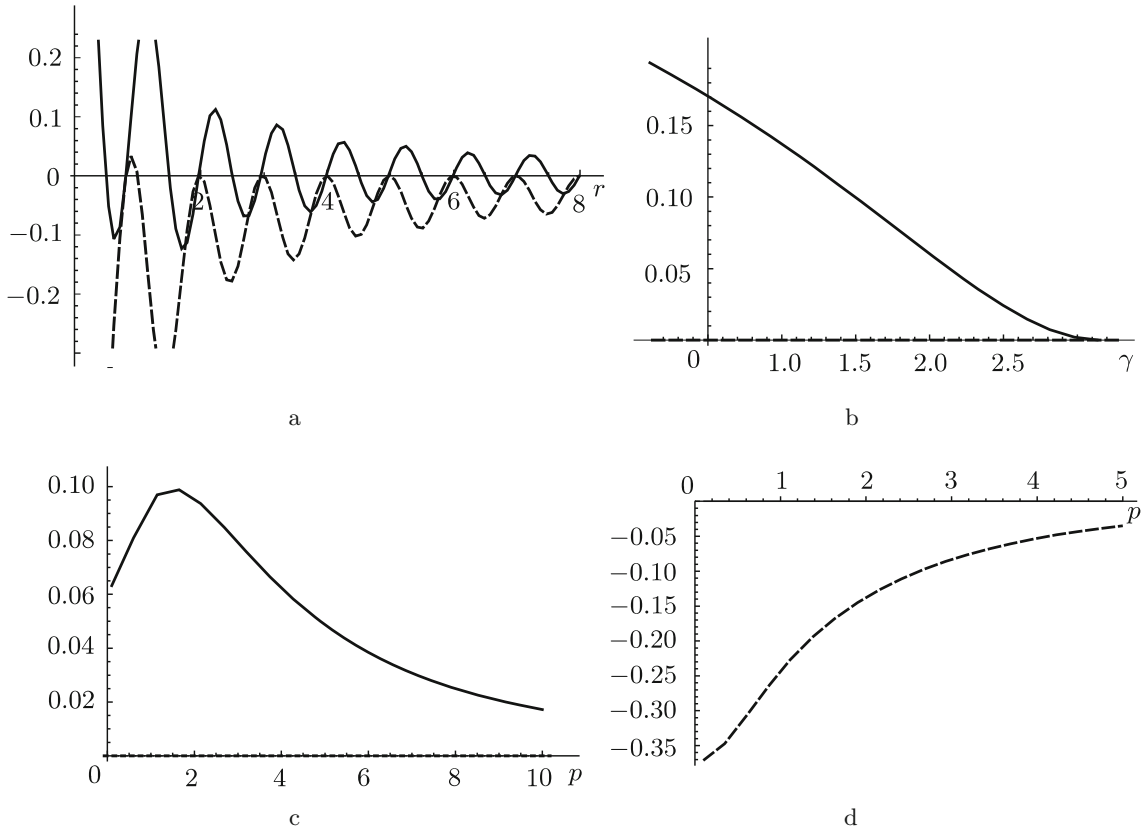

Fig. 10. (a) Dependence of the real (solid line) and imaginary (dashed line) parts of the correlation function in the momentum representation on the discrete 1-component r of the momentum. (b) Dependence of the real part of the correlation function on the deficit angle γ at $r = 2$. (c) Dependence of the real part of the correlation function in the momentum representation on the continuous 0-component p of the momentum at $r = 2$ and $\gamma = \pi/2$. (d) Dependence of the imaginary part of the correlation function in the momentum representation on p at $r = 2.5$.

p of the momentum at the integer value $r = 2$ and the fixed deficit angle $\gamma = \pi/2$. In Fig. 10d, we show the dependence of the imaginary part of the correlation function on p at noninteger $r = 2.5$.

The analogous dependences in the two-geodesic approximation compared with the dependences in Fig. 10 are shown in Fig. 11. The thin lines correspond to the shortest-geodesic approximation, and the thick lines correspond to the two-geodesic approximation. It can be seen (see Fig. 11a) that the imaginary part of the correlation function is zero at integer points.

4.3. Moving quantized conical defect. In this section, we consider a moving particle with a deficit angle $2\gamma = \pi$ at different $\psi_0 \geq 0$. The corresponding identification vector has the coordinates (see Fig. 12a)

$$\tau_0 = -2 \arctan \tanh \psi_0, \qquad \phi_0 = -2 \arctan \frac{1}{\tanh \psi_0}.$$

Here, we analyze the momentum representation of the correlation function in the case of one moving particle:

$$\mathcal{G}_{\text{1-spiral}}(p, \frac{2\pi}{L_0} r) = \int_0^{L_0} \frac{d\phi}{L_0} \int_{-\infty}^{\infty} \frac{dt}{2\pi} e^{-itp - i\phi(2\pi/L_0)r} \langle \Phi_0(\tau, \phi) \Phi_0(0, 0) \rangle_{\text{1-spiral}}, \tag{25}$$

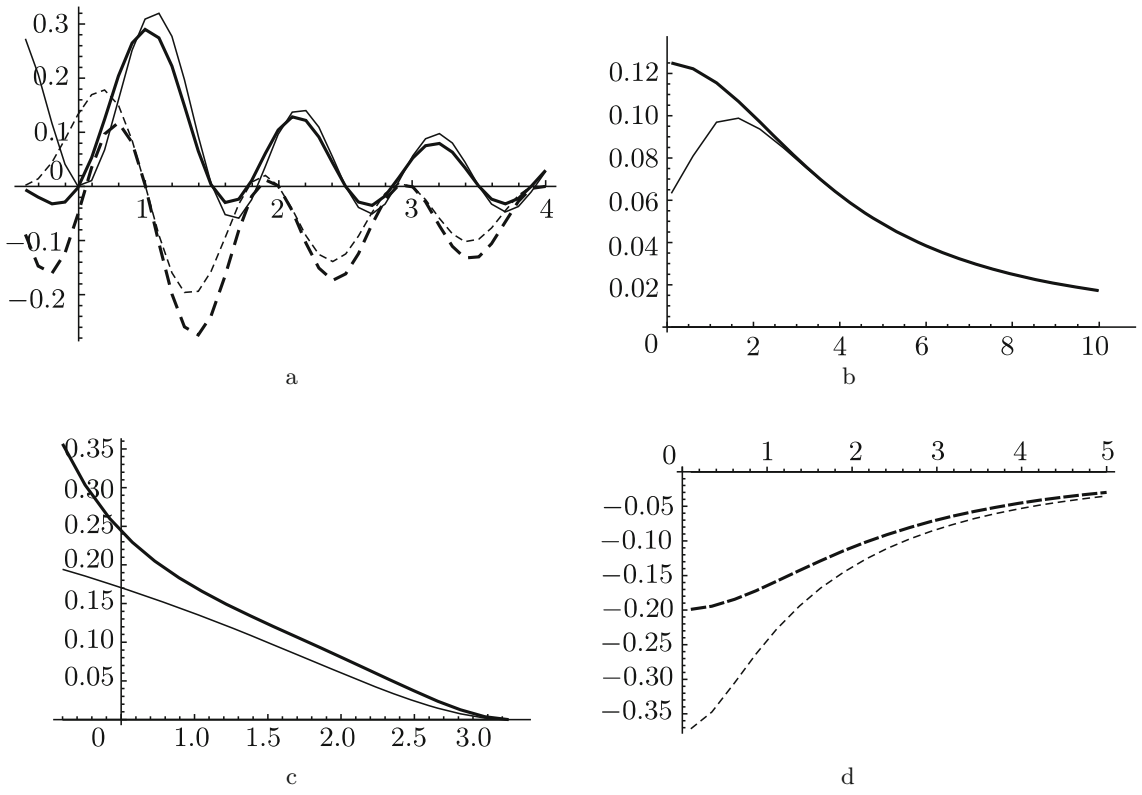

Fig. 11. Dependence of the real (solid line) and imaginary (dashed line) parts of the correlation function on the variables r, γ, and p in the shortest-geodesic approximation shown in Fig. 10 (thin lines in all pictures) compared with the same dependence in the two-geodesic approximation (thick lines).

where $L_0 = |\phi_0 - \tau_0|$. We use the two-geodesic approximation. The correlation functions in this case are defined as

$$\langle\Phi_0(\tau,\phi)\Phi_0(0,0) >_{\text{1-spiral}} = \langle\Phi_0(\tau,\phi)\Phi_0(0,0)\rangle + \langle\Phi_0(\tau_0,\phi_0)\Phi_0(\tau,\phi)\rangle.$$

The calculation results are shown in Fig. 12.

4.4. Entanglement entropy. Our result can also be used to study the holographic entanglement entropy [18]. It is known that in two-dimensional conformal field theory, the correlation functions of operators with zero conformal weight coincide with the entanglement entropy up to normalization, which allows regarding them as a measure of that entropy. A remarkable property of the entanglement entropy is its universal behavior [19]. The evolution of the entanglement entropy in a two-dimensional quantum system after a quench was analyzed in [20]. In the general case, calculating the entanglement entropy in quantum field theory is a very complicated problem because it involves calculating traces of the density matrix. A formula for the entanglement entropy in an arbitrary holographic field theory was proposed in [21]. This formula can be generalized to the case of nonconformal field theories whose symmetry is broken as a result of defects. In this case, the entanglement entropy is

$$A(m_{[\phi,\psi]}) \sim \min\{\log(2(1-\cos(\phi-\psi))),\, \log(2(1-\cos(\phi^*-\psi)))\}.$$

Here, as in [21], the entanglement entropy of the interval $[\phi,\psi]$ (the arc $[\phi,\psi]$) is the minimal surface relying on the interval $[\phi,\psi]$. The mutual information of two intervals $[\phi_1,\psi_1]$ and $[\phi_2,\psi_2]$ here must be defined as

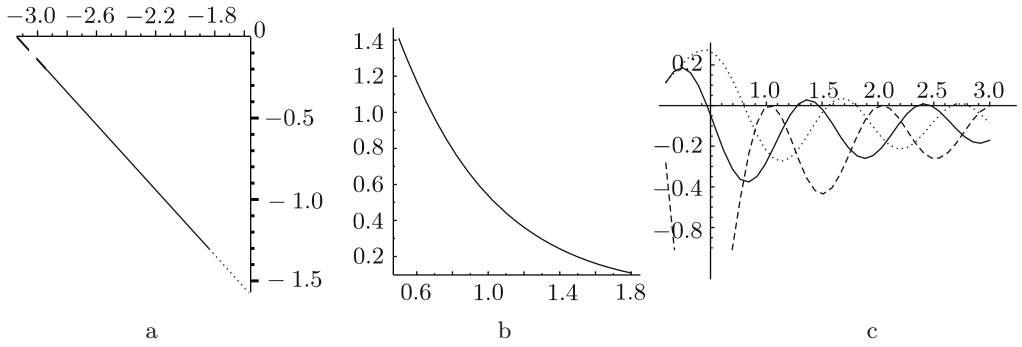

Fig. 12. (a) Identification vector (15) for $2\gamma = \pi$ and different values of ψ_0: $0 < \psi_0 < 0.1$, dashed line; $0.1 < \psi_0 < 1$, solid line; and $1 < \psi_0 < 10$, dotted line. (b) Dependence of the size of the living space on ψ_0. (c) The imaginary part of correlation function (25) for different values of ψ_0: $\psi_0 = 0.05$, dashed line; $\psi_0 = 0.5$, solid line; and $\psi_0 = 1.5$, dotted line.

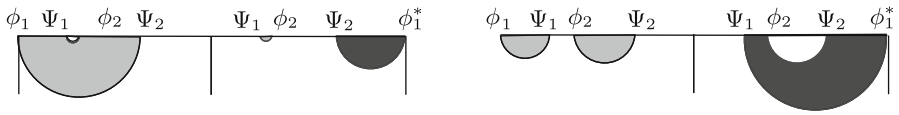

Fig. 13. Locally minimal surfaces for the boundary region.

the minimum of four quantities:

$$S_{[\phi_1,\psi_1]\cup[\phi_2,\psi_2]} = s\min\{A(m_{\rm dis}),\, A(m_{\rm con}),\, A(m^*_{\rm dis}),\, A(m^*_{\rm con})\},$$

where s is a negative constant and (see Fig. 13)

$$\begin{aligned}
A(m_{\rm dis}) &= A(m_{[\phi_1,\psi_1]}) + A(m_{[\phi_2,\psi_2]}) = \\
&= 2\ell_{\rm AdS}\log\frac{2(1-\cos(\phi_1-\psi_1))}{2} + \log\frac{1-\cos(\phi_2-\psi_2)}{2}, \\
A(m_{\rm con}) &= A(m_{[\psi_1,\phi_2]}) + A(m_{[\phi_1,\psi_2]}) = \\
&= \log\frac{1-\cos(\psi_1-\phi_2)}{2} + \log\frac{1-\cos(\phi_1-\psi_2)}{2}, \\
A(m^*_{\rm dis}) &= A(m_{[\phi_1^*,\psi_1]}) + A(m_{[\phi_2,\psi_2]}) = \\
&= \log\frac{1-\cos(\psi_1-\phi_1^*)}{2} + \log\frac{1-\cos(\psi_2-\phi_2)}{2}, \\
A(m^*_{\rm con}) &= \log\frac{1-\cos(\psi_2-\phi_1^*)}{2} + \log\frac{1-\cos(\phi_2-\psi_1)}{2}.
\end{aligned}$$

5. Conclusion

We have considered a moving conical defect in an empty AdS_3 space–time and calculated the two-point correlation function of the corresponding two-dimensional boundary quantum field theory in the shortest-geodesic approximation. We showed that the presence of the defect leads to gravitational lensing of geodesics, which in turn results in a finite number of similar terms in the Green's function of the dual

theory that correspond to winding of geodesics around the conical singularity. We showed that for special values of the deficit angle $\gamma = \pi(2n-1)/2n$, the lensing produces excitations of the domain wall type in the spectrum of the dual theory. It would be interesting to learn whether this effect is an artifact of the shortest-geodesic approximation and whether it vanishes when higher windings are taken into account.

In the model we analyzed, we studied the evolution of the entanglement entropy by analogy with previous considerations [22], [17]. It would be interesting to analyze this model for phase transitions similar to the one found in [21].

Another holographic model related to the considered topological defects was investigated in [23].

Appendix: Complexification of geodesics in global coordinates and correlation functions for timelike points

For two points on the boundary separated by a timelike interval, there is no bulk geodesic connecting them. Using the complexification of nonreturning spacelike geodesics to find the correlation functions corresponding to such points was proposed in [17]. In the Poincaré coordinates (t, x, z), these geodesics have the forms

$$z(\lambda) = \frac{1}{\sqrt{E^2 - J^2}\sinh(\lambda - \lambda_0)},$$

$$x(\lambda) = x_0 - \frac{J}{E^2 - J^2}\coth(\lambda - \lambda_0),$$

$$t(\lambda) = t_0 - \frac{E}{E^2 - J^2}\coth(\lambda - \lambda_0).$$

Here, we assume that $E^2 > J^2$. In what follows, we assume that $\lambda_0 = 0$.

To perform the complexification, the authors of [17] proposed adding a small imaginary part to the affine parameter $\lambda \to \lambda + i\beta$, and we consequently have

$$z(\lambda) = \frac{1}{\sqrt{E^2 - J^2}}\frac{\sinh\lambda\cos\beta - i\cosh\lambda\sin\beta}{\sinh^2\lambda\cos^2\beta + \cosh^2\lambda\sin^2\beta},$$

$$x(\lambda) = \frac{J}{E^2 - J^2}\frac{\sinh 2\lambda - i\sin 2\beta}{\cosh 2\lambda - \cos 2\beta},$$

$$t(\lambda) = \frac{E}{E^2 - J^2}\frac{\sinh 2\lambda - i\sin 2\beta}{\cosh 2\lambda - \cos 2\beta}.$$

We clarify how the complexification works in the global coordinates

$$\cot\tau = \sinh\mu\tanh\lambda, \tag{A.1}$$

$$\sinh\chi = \pm\cosh\mu\sinh\lambda, \tag{A.2}$$

where $\sinh\mu \equiv (E - 1/E)/2$. For definiteness, we take the plus sign in (A.2). We apply the complexification procedure to (A.1) and (A.2) and obtain

$$\cot\tau_c = \sinh\mu\tanh(\lambda + i\beta) = \sinh\mu\,\frac{\sinh 2\lambda + i\sin 2\beta}{\cosh 2\lambda + \cos 2\beta}, \tag{A.3}$$

$$\sinh\chi_c = \cosh\mu\sinh(\lambda + i\beta) = \cosh\mu(\sinh\lambda\cos\beta + i\cosh\lambda\sin\beta). \tag{A.4}$$

These formulas show that complexification in the global coordinates corresponds to complexification of the parameter s in the geodesic representation presented in [11]:

$$s \to s + i\frac{\beta}{\sqrt{\xi^2 - 1}}.$$

On the complexified geodesic, we have the relation

$$\cosh^2\lambda = \frac{|\sinh\chi_c|^2}{\cosh^2\mu} + \cos^2\beta, \quad \text{where } |\sinh\chi_c|^2 = \cosh^2\mu(\cosh^2\lambda - \cos^2\beta),$$

and the geodesic length is

$$\Delta\lambda = \operatorname{arccosh} 2\sqrt{\frac{|\sinh\chi_c|^2}{\cosh^2\mu} + \cos^2\beta} =$$

$$= 2\log\left(\sqrt{\frac{|\sinh\chi_c|^2}{\cosh^2\mu} + \cos^2\beta} + \sqrt{\frac{|\sinh\chi_c|^2}{\cosh^2\mu} - \sin^2\beta}\right).$$

Separating the divergent part, we obtain

$$L_{\text{ren}} = \lim_{|\sinh\chi_c|\to\infty}(\Delta\lambda - 2\log|\sinh\chi_c|^2) = \log\frac{4}{\cosh^2\mu}, \qquad |\sinh\chi_c|^2 = \frac{1}{\delta^2}.$$

From (A.4), we see that $\cot\tau_{\max} = \sinh\mu$, and taking this relation into account, we can write

$$L_{\text{ren}} = \log 4\sin^2\tau_{\max} = \log 2(\cos 2\tau_{\max} - 1).$$

Therefore, the correlation function is

$$G_\Delta(-\tau_{\max}; 0, \tau_{\max}, 0) = [2(\cos 2\tau_{\max}) - 1]^{-\Delta},$$

which agrees with (17).

Acknowledgments. It is our great honor to dedicate this paper to the 75th birthday of Academician A. A. Slavnov. One of the authors (I. Ya. A.) is grateful to D. Ageev for the help with numerical calculations. One of the authors (A. A. B.) is grateful to S. Dedeo and P. Saterskog for the useful discussions.

This work was supported in part by the Russian Science Foundation (Grant No. 14-11-00687, I. Ya. A., Steklov Mathematical Institute, Moscow).

REFERENCES

1. O. Aharony, S. S. Gubser, J. M. Maldacena, H. Ooguri, and Y. Oz, *Phys. Rept.*, **323**, 183–386 (2000); arXiv:hep-th/9905111v3 (1999).
2. J. Casalderrey-Solana, H. Liu, D. Mateos, K. Rajagopal, and U. A. Wiedemann, "Gauge/string duality, hot QCD, and heavy ion collisions," arXiv:1101.0618v2 [hep-th] (2011).
3. I. Ya. Aref'eva, *Phys. Usp.*, **57**, 527–555 (2014).
4. W. Witczak-Krempa, E. Sorensen, and S. Sachdev, *Nature Phys.*, **10**, 361–366 (2014); arXiv:1309.2941v2 [cond-mat.str-el] (2013).
5. G. 't Hooft, *Class. Q. Grav.*, **13**, 1023–1039 (1996); arXiv:gr-qc/9601014v1 (1996).
6. S. Deser, R. Jackiw, and G. 't Hooft, *Ann. Phys.*, **152**, 220–235 (1984).

7. M. Smolkin and S. N. Solodukhin, "Correlation functions on conical defects," arXiv:v3 [hep-th] (2014).
8. V. Balasubramanian and S. F. Ross, *Phys. Rev. D*, **61**, 044007 (2000); arXiv:hep-th/9906226v1 (1999).
9. C. A. B. Bayona, C. N. Ferreira, and V. J. V. Otoya, *Class. Q. Grav.*, **28**, 015011 (2011); arXiv:1003.5396v3 [hep-th] (2010).
10. I. Ya. Aref'eva, "Colliding hadrons as cosmic membranes and possible signatures of lost momentum," arXiv: 1007.4777v1 [hep-th] (2010).
11. H.-J. Matschull and M. Welling, *Class. Q. Grav.*, **15**, 2981–3030 (1998); arXiv:gr-qc/9708054v2 (1997).
12. H.-J. Matschull, *Class. Q. Grav.*, **16**, 1069–1095 (1999); arXiv:gr-qc/9809087v3 (1998).
13. S. Holst and H.-J. Matschull, *Class. Q. Grav.*, **16**, 3095–3131 (1999); arXiv:gr-qc/9905030v1 (1999).
14. S. W. Hawking and G. F. R. Ellis, *The Large Scale Structure of Space–Time* (Cambridge Monogr. Math. Phys., Vol. 1), Cambridge Univ. Press, Cambridge (1973).
15. S. DeDeo and J. R. Gott, *Phys. Rev. D*, **66**, 084020 (2002); Erratum, **67**, 069902 (2003); arXiv:gr-qc/0212118v1 (2002).
16. I. Ya. Aref'eva and I. V. Volovich, *Phys. Lett. B*, **433**, 49–55 (1998); arXiv:hep-th/9804182v2 (1998).
17. V. Balasubramanian, A. Bernamonti, B. Craps, V. Keränen, E. Keski-Vakkuri, B. Müller, L. Thorlacius, and J. Vanhoof, *JHEP*, **1304**, 069 (2013); arXiv:1212.6066v2 [hep-th] (2012).
18. S. Ryu and T. Takayanagi, *JHEP*, **0608**, 045 (2006); arXiv:hep-th/0605073v3 (2006).
19. P. Calabrese and J. L. Cardy, *J. Stat. Mech.*, **0406**, 002 (2004); arXiv:hep-th/0405152v3 (2004).
20. P. Calabrese and J. L. Cardy, *J. Stat. Mech.*, **0504**, 010 (2005); arXiv:cond-mat/0503393v1 (2005).
21. M. Headrick, *Phys. Rev. D*, **82**, 126010 (2010); arXiv:1006.0047v3 [hep-th] (2010).
22. J. Abajo-Arrastia, J. Aparicio, and E. L'opez, *JHEP*, **1011**, 149 (2010); arXiv:1006.4090v1 [hep-th] (2010).
23. V. Balasubramanian, P. Hayden, A. Maloney, D. Marolf, and S. F. Ross, "Multiboundary wormholes and holographic entanglement," arXiv:1406.2663v2 [hep-th] (2014).